Journal of Alloys and Compounds 503 (2010) 431–435

Contents lists available at ScienceDirect

Journal of Alloys and Compounds

journal homepage: www.elsevier.com/locate/jallcom

Synthesis, mechanical and magnetic properties of transition metals-doped $Ca_3Co_{3.8}M_{0.2}O_9$

S. Pinitsoontorn[a,*], N. Lerssongkram[a], A. Harnwunggmoung[b], K. Kurosaki[b], S. Yamanaka[b]

[a] Department of Physics, Faculty of Science, Khon Kaen University, Khon Kaen 40002, Thailand
[b] Graduate School of Engineering, Osaka University, Suita 565-0871, Japan

ARTICLE INFO

Article history:
Received 18 March 2010
Received in revised form 30 April 2010
Accepted 2 May 2010
Available online 11 May 2010

Keywords:
$Ca_3Co_4O_9$
Thermoelectric
Mechanical properties
Magnetic measurements
Sol–gel synthesis

ABSTRACT

We report the synthesis of a thermoelectric oxide $Ca_3Co_4O_9$ using a sol–gel method with polyvinyl alcohol as the dispersion agent. The transition metals (Cr, Fe, Ni, Cu and Zn) were doped at the Co-site to form $Ca_3Co_{3.8}M_{0.2}O_9$. The single phases of the doped $Ca_3Co_{3.8}M_{0.2}O_9$ were confirmed by thermogravimetric and differential thermal analysis, and X-ray diffraction patterns. Relatively high porosity was observed in scanning electron micrographs. The density of the samples was the highest for Cu-doped $Ca_3Co_{3.8}M_{0.2}O_9$ (78% of the theoretical density). The Young's modulus and shear modulus measured by the sound velocity method were found to be in the order of tens of GPa, and also found to be highly correlated to the density of the samples. The magnetic properties of the transition metals-doped $Ca_3Co_{3.8}M_{0.2}O_9$ were found to be insensitive to the doping and all sintered samples showed paramagnetic behaviour, with susceptibility of $\sim 10^{-6}$ emu/(Oe g), at room temperature.

1. Introduction

Thermoelectric materials are well known for directly converting heat to electrical power. The conversion efficiency of thermoelectric materials depends on the dimensionless figure of merit, ZT defined as $ZT = S^2/\rho\kappa$, where S is the Seebeck coefficient, ρ is the electrical resistivity and κ is the thermal conductivity. For practical use, a thermoelectric material should exhibit $ZT > 1$ [1].

In recent years, thermoelectric oxide materials have become a popular research topic due to their good thermal and chemical stability in air at high temperature in comparison to intermetallic thermoelectric compounds, such as Bi_2Te_3 [2]. In particular, $Ca_3Co_4O_9$ has become a strong candidate for high temperature applications. The crystal structure of $Ca_3Co_4O_9$ is a misfit-layered structure consisting of two monoclinic subsystems, namely the CaO–CoO–CaO rocksalt-type layer and the CdI_2-type CoO_2 layer stacked along the c-axis direction [3]. It was reported that the thermoelectric properties along the ab-plane were promisingly good with the ZT close to unity in its single crystal or thin film forms [4,5]. However, for polycrystalline materials, the reported ZT were still too low for practical applications [6–10].

There have been a number of attempts to improve the thermoelectric properties of polycrystalline $Ca_3Co_4O_9$, including adding texture along the c-axis [11,12], improving the sintering method [13], or inventing the novel synthesis method [14–16]. $Ca_3Co_4O_9$ was generally prepared by a conventional solid state reaction starting from a mixture of calcium carbonate and cobalt oxide [3,10]. However, some reports show that the $Ca_3Co_4O_9$ samples synthesized by the sol–gel method have a finer grain size and more uniform size distribution, which are believed to be an important key figures to improve thermoelectric properties [14,16].

The alternative route to improve the thermoelectric properties is to partially substitute some elements into $Ca_3Co_4O_9$ to simultaneously reduce electrical resistivity and thermal conductivity. The substitution can take place either at the Ca-site (Na [17], Bi [18], Y [8], Sr [7], Ag [19], rare earth [20]) or at the Co-site (Ga [9], Mn [6,10,21,22], Fe [10,22,23], Cu [10,22]) In the case of the transition metals-doped $Ca_3Co_{4-x}M_xO_9$ materials, it was reported that partial substitution ($x = 0.05$ and 0.1) of Mn, Fe or Cu at Co-site shows a strong improvement of ZT, with the largest ZT of 0.4 at 1000 K [10,22].

For practical applications, such as thermoelectric modules, not only high thermoelectric properties of $Ca_3Co_4O_9$ are required, but other properties need to be optimized. Mechanical properties, for examples, need to be sufficiently strong to withstand loads during module life times. Magnetic properties, on the other hand, need to be optimized in the transition metals doping case, since doping transition metals into oxide materials can introduce ferromagnetic phases [24] which in turn might have an effect on electron transport of thermoelectric materials [25,26].

In this paper, we report synthesis of polycrystalline $Ca_3Co_{4-x}M_xO_9$ by a polyvinyl alcohol sol–gel method. We

* Corresponding author.
E-mail address: psupree@kku.ac.th (S. Pinitsoontorn).

0925-8388/$ – see front matter © 2010 Elsevier B.V. All rights reserved.
doi:10.1016/j.jallcom.2010.05.027

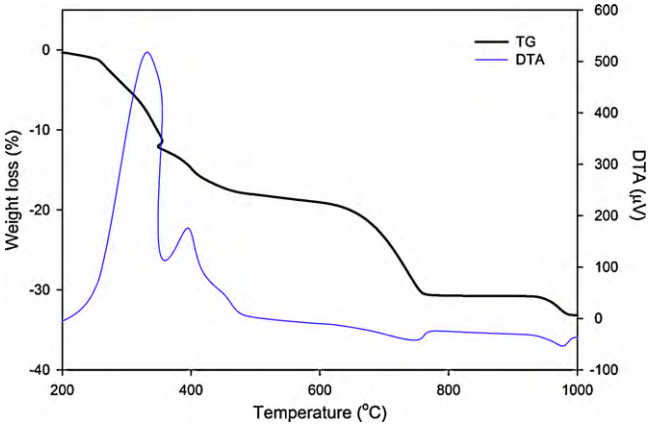

Fig. 1. TG-DTA curves of the CCO349 precursor.

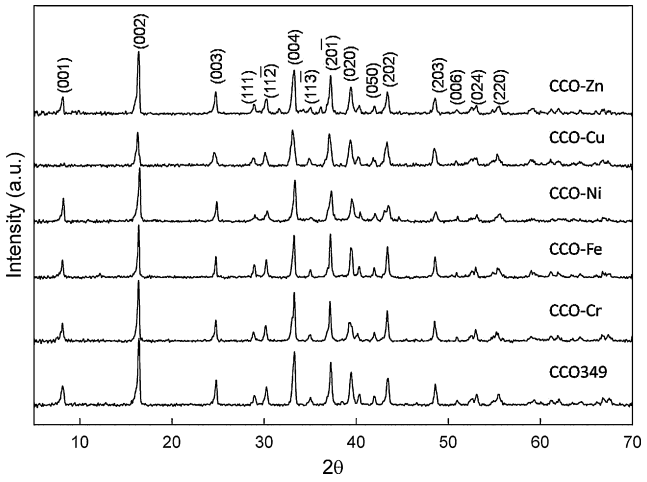

Fig. 2. Powder XRD patterns for the calcined CCO349 and CCO–M samples.

partially substitute cobalt with a higher content ($x = 0.2$) of the other transition metals (M = Cr, Fe, Ni, Zn, Cu) than previously reported [10,21,22], and we focus on the mechanical and magnetic properties at room temperature.

2. Experimental details

$Ca_3Co_4O_9$ and $Ca_3Co_{3.8}M_{0.2}O_9$ (M = Cr, Fe, Ni, Cu, Zn) powders were prepared by a sol–gel method using polyvinyl alcohol (PVA) as a dispersant agent. A mixture of $Ca(NO_3)_2$, $Co(NO_3)_2$, $Cr(NO_3)_3$, $Fe(NO_3)_3$, $NiNO_3$, CuO and $ZnNO_3$ in a stoichiometric ratio was dissolved and thoroughly stirred in a citric acid solution. A solution of 5 wt% PVA was added and the mixture was stirred at a temperature of 80–100 °C until the gel was formed. The gel was further heated to obtain a precursor by autocombustion. The precursor was ground and calcined at 800 °C for 4 h in air. The powders were then reground and uniaxially pressed at 400 MPa to form pellets which were sintered at 890 °C for 4 h in air. For convenience in the following texts, the $Ca_3Co_{3.8}M_{0.2}O_9$ sample without transition metals doping is referred to as CCO349 where as the others are shortened as CCO–M (M = Cr, Fe, Ni, Cu and Zn).

Thermogravimetry (TG) and differential thermal analysis (DTA) of the gel was carried out from room temperature to 1000 °C. X-ray diffraction (XRD) analysis of both calcined powders and sintered samples was carried out to verify the phase identity using an XRD diffractometer with Cu Kα radiation. Morphology and chemical composition of the samples were characterized using a scanning electron microscope (SEM) equipped with an energy dispersive X-ray spectroscopy (EDS). The densities of the samples were calculated from the mass and dimension measurements. For mechanical properties, the longitudinal and shear sound velocities of the samples were measured by an ultrasonic pulse echo method at room temperature to evaluate the shear modulus, Young's modulus, compressibility and Poisson's ratio. Magnetic properties of the samples were measured from a vibrating sample magnetometer (VSM) at room temperature.

3. Results and discussion

The TG and DTA curves of the CCO349 precursor are shown in Fig. 1. From the DTA curve, the extremely high endothermic peak at 332 °C can be observed. This corresponds to a rapid weight loss of 12% in the TG curve which can be attributed to the autocombustion of the remaining organic species (nitric acid, citric acid and PVA). The other endothermic peaks at 395 °C and 455 °C are associated with the decomposition of the PVA complex to Co_3O_4 and $CaCO_3$. The exothermic peak at 747 °C corresponds to another weight loss of 12% attributed to the reaction of Co_3O_4 and $CaCO_3$ to form the $Ca_3Co_4O_9$ phase. The plateau in the TG curve clearly observed between 772 °C and 940 °C also confirms the formation of the $Ca_3Co_4O_9$ single phase in this temperature range. Above 940 °C, the TG curve shows a small weight loss corresponding to a small exothermic peak, which indicates a transformation of the $Co_3C_4O_9$ phase to the $Ca_3Co_2O_6$ phase.

The XRD patterns of the calcined samples are shown in Fig. 2. The peak positions of all samples can be matched with the standard JCPDS card (21-139) of $Ca_9Co_{12}O_{28}$, and the diffraction peaks in Fig. 2 are indexed according to the previously reported results [3,8]. The XRD patterns show no secondary phase of any CCO–M samples indicating that the single phase of the transition metals-doped CCO–M was formed. The slight shift of the XRD peaks in the CCO–M samples in comparison to the CCO349 confirms that transition metals were indeed substituted in the $Ca_3Co_4O_9$ structure [8,27].

Fig. 3 shows the XRD patterns of the sintered samples. The peak positions are insignificantly different from the calcined samples but the intensities of the peaks are different. The intensities of the (0 0 l) peaks are much stronger compared to the other ($h\,k\,l$) peaks, indicating a strong preferred orientation along the (0 0 l) plane of the CCO349 and CCO–M pellets. This is believed to be a result of an induced texture from the uniaxial pressing, as was reported previously [11,12].

The pressed surface of the sintered CCO349 and CCO–M samples are illustrated in the SEM images as shown in Fig. 4. It can be seen that no obvious second phases are present and all samples contain spherical-like grains, particularly the CCO–Cr samples in Fig. 4(a). No sheet-like or plate-like grains, as reported in the textured $Ca_3Co_4O_9$ [11,12], are observed in any samples. The grain size for all cases can be estimated to be in the range of 1–5 μm, although the particle sizes of the calcined samples are hundreds of nanometers. For the CCO–Ni (Fig. 4(a)) and CCO–Zn (Fig. 4(b)) samples, some grains appear to be interconnected with neighbour grains

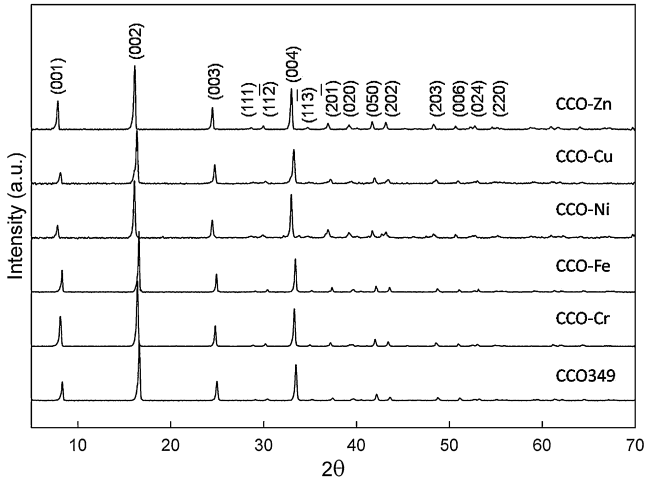

Fig. 3. XRD patterns for sintered CCO349 and CCO–M samples indicating *c*-axis preferred orientation.

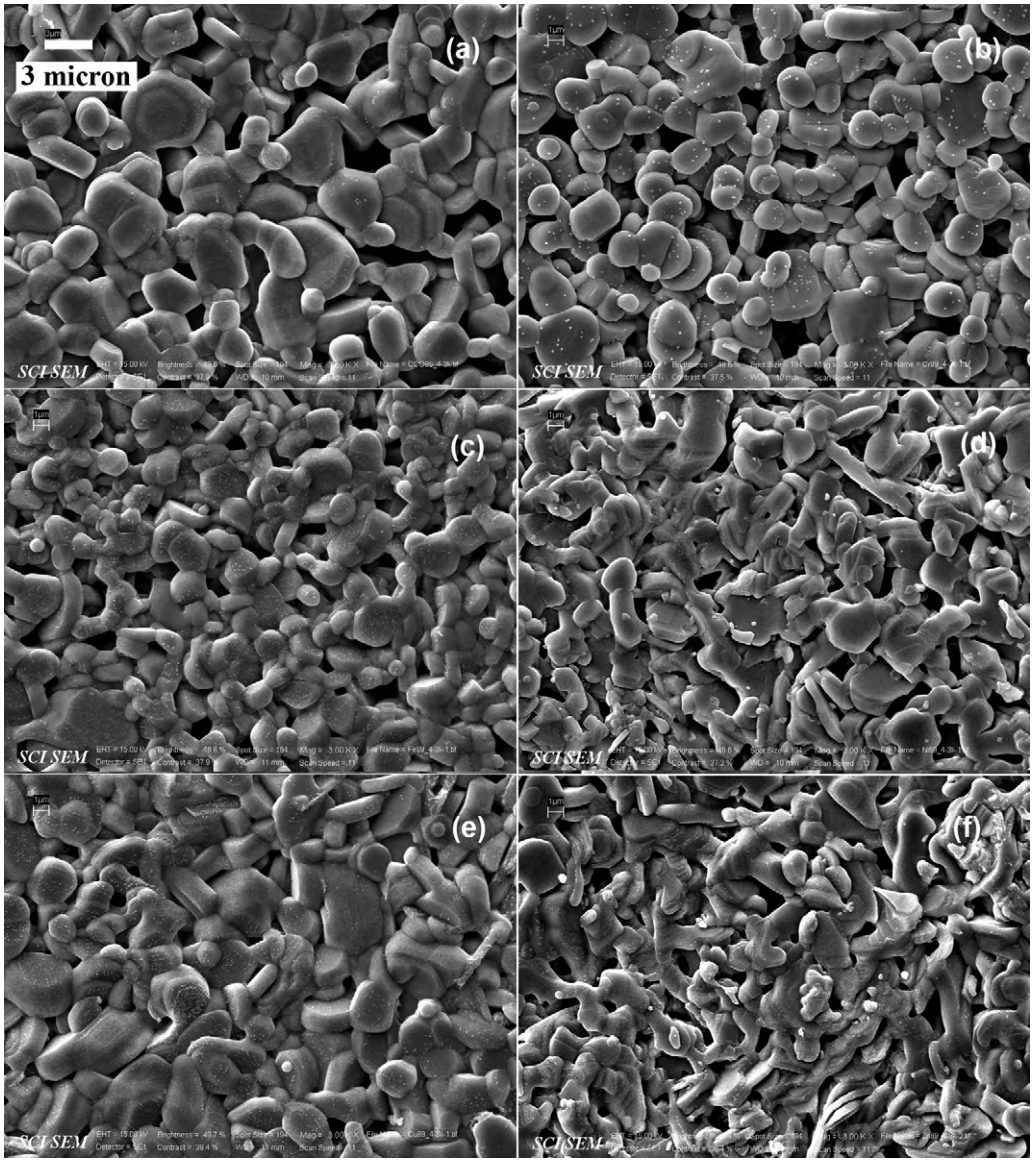

Fig. 4. SEM micrographs of the sintered samples of (a) CCO349, (b) CCO–Cr, (c) CCO–Fe, (d) CCO–Ni, (e) CCO–Cu, (f) CCO–Zn.

resulting in an elongated shape, and individual grain boundaries are difficult to distinguish. It can be clearly seen that all samples still contain significant pores, particularly for the undoped CCO349 samples (Fig. 4(a)). The porosity results in the low bulk density of the CCO349 samples of 3.22 g/cm^3, only about 65% of the theoretical density of $Ca_3Co_4O_9$. Doping transition metals results in a decrease in porosity as shown in Fig. 4(b–f). In particular, the CCO–Cu appears to be the densest among all samples, with a density of 3.76 g/cm^3, about 76% of the theoretical density. The bulk densities of the CCO349 and CCO–M samples are summarized in Table 1. Furthermore, the chemical compositions of all samples were verified by EDS. It was confirmed that the chemical compositions of the doped samples correspond to the stoichiometric ratios. The composition distributions are uniform, no phase segregations were observed, whether within grains or at the grain boundaries.

For the mechanical properties of the sintered samples, the shear modulus (G), Young's modulus (E), compressibility (β), and Poisson's ratio (υ) can be written in terms of the longitudinal sound

Table 1
Summary of the mechanical and magnetic properties of CCO349 and CCO–M (M = Cr, Fe, Ni, Cu, Zn).

Sample	Density (g/cm^3)	Young's modulus (GPa)	Shear modulus (GPa)	Compressibility (GPa^{-1})	Magnetization at 10 kOe (emu/g)		Susceptibility (10^{-6} emu/(Oe g))	
					Sintered	Calcined	Sintered	Calcined
CCO349	3.22	33.1	13.3	0.0453	0.085	0.125	8.70	32.0
CCO–Cr	3.44	37.7	15.1	0.0398	0.076	0.089	7.70	18.1
CCO–Fe	3.53	43.9	17.5	0.0342	0.105	0.077	10.6	14.9
CCO–Ni	3.47	35.5	14.2	0.0423	0.093	0.105	9.57	34.2
CCO–Cu	3.76	61.5	24.6	0.0244	0.070	0.116	7.26	71.4
CCO–Zn	3.44	39.6	15.8	0.0379	0.073	0.088	7.60	16.1

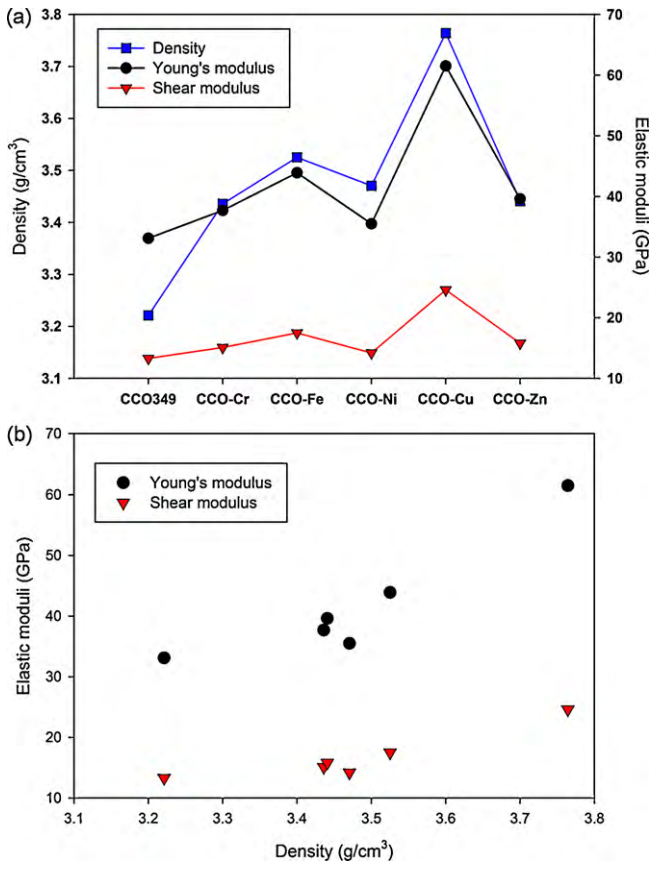

Fig. 5. (a) Densities and elastic moduli of the sintered CCO349 and CCO–M samples and (b) a plot of elastic moduli versus sample density.

velocity (V_L) and shear sound velocity (V_S) as follows [28,29]:

$$E = \frac{\rho V_S^2(3V_L^2 - 4V_S^2)}{V_L^2 - V_S^2} \quad (1)$$

$$G = \rho V_S^2 \quad (2)$$

$$\beta = \frac{1}{\rho(V_L^2 - (4/3)V_S^2)} \quad (3)$$

$$\upsilon = \frac{1}{2}\frac{V_L^2 - 2V_S^2}{V_L^2 - V_S^2} \quad (4)$$

The mechanical properties of the samples are summarized as shown in Table 1. The Poisson's ratios are calculated to be 0.25 for all samples. The elastic moduli of CCO349 are found to be lower than their related thermoelectric oxide $Na_{1.5}Co_2O_4$ [28]. The Young's and shear moduli are 33.1 GPa and 13.3 GPa compared to those of 49.8 GPa and 19.9 GPa for $NaCo_2O_4$. This is believed to be a result of the low density of our sample (~65% of theoretical density for our sample compared to ~79% for $NaCo_2O_4$ [28]. Fig. 5(a) plots the density and the elastic moduli of the CCO349 and the doped CCO–M samples. It can be seen that the transition metals-doped samples show higher elastic moduli, which are highly correlated to the bulk density. The CCO–Cu sample exhibits the highest Young's and shear moduli of 61.5 GPa and 24.6 GPa, which corresponds to its highest density of 3.76 g/cm^3. The result agrees well with the micrograph in Fig. 4(e) where the grains of CCO–CU are the densest with relatively few pores. The correlation between the elastic moduli and the bulk density is illustrated in Fig. 5(b). Thus, it is assumed that the mechanical properties of $Ca_3Co_4O_9$ can be improved with a denser sample which can be achieved by a thermoforging process [11] or spark plasma sintering [13].

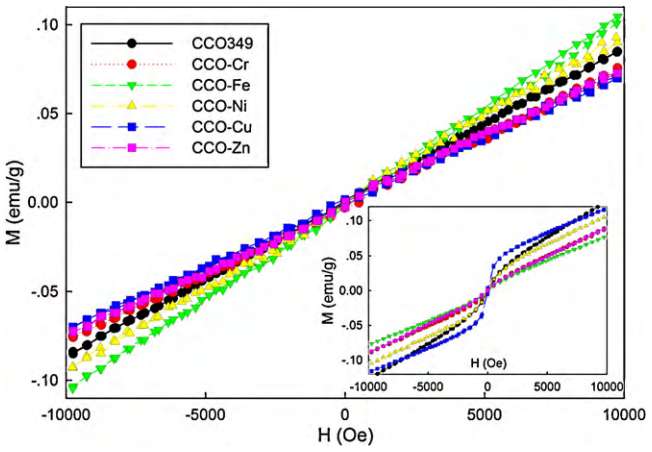

Fig. 6. A plot of the magnetization versus the external field of the sintered (calcined: inset) CCO349 and CCO–M samples.

The magnetization curves of the sintered samples are shown in Fig. 6. The magnetization curves versus the external field can be represented as straight lines with the susceptibility in the order of 10^{-6} emu/(Oe g) and the magnetization of ~10^{-2} emu/g at ±10 kOe. Thus, the magnetic measurement shows that the sintered samples behave as paramagnetic materials and the doping of transition metals at Co-sites has no significant effect on the magnetic behaviour. Moreover, the measurements were carried out at room temperature, and thus the paramagnetic phase of the sintered samples can be maintained up to the application temperature range (~1000 K). However, the calcined powders of all samples show different magnetic behaviour (inset of Fig. 6.). The curves of magnetization versus applied field are not straight lines but more superparamagnetic *S*-like curves, particularly at the fields below 3000 Oe. The highest susceptibility and magnetization of the calcined powders belong to CCO–Cu (71.4×10^{-6} emu/(Oe g)) and CCO349 (0.125 emu/g), respectively. The superparamagnetic behaviour of the calcined powders could be accounted to the partial incomplete formation of the $Ca_3Co_4O_9$ phase, and also the effect of the nanosize of the calcined powders, which results in zero remanence when the applied field is removed. Nonetheless, further confirmation on this issue is necessary. The magnetic properties of both calcined and sintered samples are summarized in Table 1.

4. Conclusions

$Ca_3Co_4O_9$ ceramics were synthesized by a sol–gel method using PVA as a dispersion agent. The transition metals (Cr, Fe, Ni, Cu and Zn) were successfully substituted at the Co-sites. The XRD patterns and SEM micrographs show supporting evidence of the single phase formation. The uniaxial pressure has induced grain orientation along the *c*-axis. The mechanical properties are found to be dependent on the sample density, and can be improved by advanced forming and sintering process. The doping of transition metals into the $Ca_3Co_4O_9$ structure has no significant effect on the magnetic behaviour. All sintered samples show paramagnetic behaviour which can be maintained up to the application temperature range.

Acknowledgements

This project funding was supported by the Integrated Nanotechnology Research Center, Khon Kaen University, Thailand. The authors would like to thank Assoc. Prof. Santi Maensiri for his excellent suggestions for the manuscript.

References

[1] T.M. Tritt, M.A. Subramanian, MRS Bull. 31 (2006) 188–194.
[2] K. Koumoto, I. Terasaki, R. Funahashi, MRS Bull. 31 (2006) 206–210.
[3] A.C. Masset, C. Michel, A. Maignan, M. Hervieu, O. Toulemonde, F. Studer, B. Raveau, Phys. Rev. B 62 (2000) 166–175.
[4] H. Ohta, K. Sugiura, K. Koumoto, Inorg. Chem. 47 (2008) 8429–8436.
[5] M. Shikano, R. Funahashi, Appl. Phys. Lett. 82 (2003) 1851–1853.
[6] D. Li, X.Y. Qin, Y.J. Gu, J. Zhang, Solid State Commun. 134 (2005) 235–238.
[7] S. Li, R. Funahashi, I. Matsubara, H. Yamada, K. Ueno, S. Sodeoka, Ceram. Int. 27 (2001) 321–324.
[8] H.Q. Liu, Y. Song, S.N. Zhang, X.B. Zhao, F.R. Wang, J. Phys. Chem. Solids 70 (2009) 600–603.
[9] N.V. Nong, C.-J. Liu, M. Ohtaki, J. Alloys Compd. 491 (2010) 53–56.
[10] Y. Wang, Y. Sui, P. Ren, L. Wang, X.J. Wang, W.H. Su, H.J. Fan, Chem. Mater. 22 (2010) 1155–1163.
[11] M. Prevel, S. Lemonnier, Y. Klein, S. Hebert, D. Chateigner, B. Ouladdiaf, J.G. Noudem, J. Appl. Phys. 98 (2005) 093706.
[12] Y.Q. Zhou, I. Matsubara, S. Horii, T. Takeuchi, R. Funahashi, M. Shikano, J. Shimoyama, K. Kishio, W. Shin, N. Izu, N. Murayama, J. Appl. Phys. 93 (2003) 2653–2658.
[13] Y.H. Liu, Y.H. Lin, Z. Shi, C.W. Nan, Z.J. Shen, J. Am. Ceram. Soc. 88 (2005) 1337–1340.
[14] S. Katsuyama, Y. Takiguchi, M. Ito, J. Mater. Sci. 43 (2008) 3553–3559.
[15] M. Sopicka-Lizer, P. Smaczynski, K. Kozlowska, E. Bobrowska-Grzesik, J. Plewa, H. Altenburg, J. Eur. Ceram. Soc. 25 (2005) 1997–2001.
[16] Y.F. Zhang, J.X. Zhang, Q.M. Lu, Q.Y. Zhang, Mater. Lett. 60 (2006) 2443–2446.
[17] J. Nan, J. Wu, Y. Deng, C.W. Nan, J. Eur. Ceram. Soc. 23 (2003) 859–863.
[18] G.J. Xu, R. Funahashi, M. Shikano, I. Matsubara, Y.Q. Zhou, Appl. Phys. Lett. 80 (2002) 3760–3762.
[19] Y. Wang, Y. Sui, J. Cheng, X.J. Wang, J.P. Miao, Z.G. Liu, Z.N. Qian, W.H. Su, J. Alloys Compd. 448 (2008) 1–5.
[20] M. Prevel, O. Perez, J.G. Noudem, Solid State Sci. 9 (2007) 231–235.
[21] J.L. Chen, Y.S. Liu, C.-J. Liu, L.C. Huang, C.L. Dong, S.S. Chen, C.L. Chang, J. Phys. D: Appl. Phys. 42 (2009) 135418.
[22] Y. Wang, Y. Sui, X. Wang, W. Sui, X. Liu, J. Appl. Phys. 107 (2010) 033708.
[23] C.-J. Liu, L.C. Huang, J.S. Wang, Appl. Phys. Lett. 89 (2006) 135418.
[24] S. Maensiri, J. Sreesongmuang, C. Thomas, J. Klinkaewnarong, J. Magn. Magn. Mater. 301 (2006) 422–432.
[25] P. Limelette, J.C. Soret, H. Muguerra, D. Grebille, Phys. Rev. B 77 (2008) 245123.
[26] J. Sugiyama, C. Xia, T. Tani, Phys. Rev. B 67 (2003) 104410.
[27] H.Q. Liu, X.B. Zhao, F. Liu, Y. Song, Q. Sun, T.J. Zhu, F.P. Wang, J. Mater. Sci. 43 (2008) 6933–6937.
[28] T. Seetawan, V. Amornkitbamrung, T. Burinprakhon, S. Maensiri, K. Kurosaki, H. Muta, M. Uno, S. Yamanaka, J. Alloys Compd. 403 (2005) 308–311.
[29] S. Yamanaka, T. Maekawa, H. Muta, T. Matsuda, S. Kobayashi, K. Kurosaki, J. Alloys Compd. 381 (2004) 295–300.